Proceedings of the ASME 2017 International Mechanical Engineering Congress and Exposition
IMECE2017
November 3-9, 2017, Tampa, Florida, USA

IMECE2017-71856

NUMERICAL INVESTIGATION OF THE INFLUENCE OF DIFFERENT WORK DISTRIBUTIONS ON THE PERFORMANCE OF AXIAL FANS FOR AUTOMOTIVE COOLING APPLICATIONS

Philipp Epple
Coburg University of Applied Sciences
Department of Mechanical Engineering
Coburg, Germany

Alexander Porzelt
Coburg University of Applied Sciences
Department of Mechanical Engineering
Coburg, Germany

Stefan Gast
Coburg University of Applied Sciences
Department of Mechanical Engineering
Coburg, Germany

Corresponding author: philipp.epple@hs-coburg.de

ABSTRACT

In this work the influence of different radial work distributions on the performance of low pressure axial fans for automotive cooling purposes was investigated. The general standard solution in the design of axial fans is to assume constant work distribution (free vortex design). This also leads to a constant meridional flow velocity and thus makes the calculations for the design rather simple. To fulfill the constant work assumption, however, a high swirl component of the absolute outlet flow velocity results near the hub. Assuming the incoming airflow to be swirl-free, this means that the flow near the hub must be strongly deflected, leading to a very high blade load in this area and to very long chords. Thus, the assumption of constant radial work distribution leads to a high risk of flow separation near the hub, especially for low pressure cooling fans, where a small hub to shroud diameter ratio is needed in order to achieve higher flow rates.

Furthermore, in fan applications, often the total-to-static pressure and total-to-static efficiency are the relevant design parameters, and not the total-to-total pressure and the total-to-total efficiency. In order to address these issues, linear and parabolic non-constant work distributions were investigated. These distributions were parametrized and for each work distribution a series of designs was created with the airfoil theory method. These designs were computed with the commercial Navier-Stokes-Solver STAR CCM+ and the results were analyzed in detail. As an application example a series of fans for a Formula Student racing cars cooling applications was developed.

With this method, it was possible to achieve smaller hub to shroud diameter ratios, higher flow rates and better total-to-static efficiencies. The result was a new series of fans with improved cooling properties for automotive applications. These new fans, the design method and the results are presented in detail in this work.

NOMENCLATURE

δ	= diameter coefficient
σ	= speed coefficient
d	= diameter
$\dot{v}$	= flow rate
Y	= specific work
n	= rotational speed
p	= pressure
ρ	= density
c, w, u	= absolute, relative and circumferential velocity
r	= radius
ω	= angular velocity
P	= power
η	= efficiency
l	= chord length

t = spacing
c_l = lift coefficient
w_∞ = vectorially averaged relative velocity
β_∞ = angle of w_∞
ε = drag/lift ratio
z = number of blades
Re = Reynolds number
ν = kinematic viscosity

Subscripts

1 = inlet of the rotor
2 = outlet of the rotor
s = static
t = total
t-s = total-to-static
u = circumferential component
m = meridional component
hyd = hydraulic

INTRODUCTION

Low pressure axial fans usually have a small number of blades with relatively large gaps in between, i.e. a low solidity. Due to these gaps the blades behave more like isolated airfoils, rather than forming stream passages, which is the usual way to look at turbomachinery rotors. For this reason, the blades of low pressure axial fans are commonly designed using the airfoil approach instead of the streamline theory. Both approaches assume that the fluid flowing through the rotor has no radial velocity component. This means that the centrifugal force and the pressure forces must be balance each other at every radius. The Euler equation provides a relation between the total pressure or work and the velocities. Thus, the work can be specified and the velocity components which in turn determine the blade angles can be calculated by solving the radial equilibrium equation. During the design of an axial fan for a Formula Student racing car engine cooling system it was found, that a constant work distribution does not result in optimal designs for the present application. It resulted in a very large flow angle difference between the inlet and the outlet of the rotor near the hub. This strong flow deflection raises the risk of flow separation, which leads to poor efficiency. [1] [2]

Using the airfoil approach for the blade design, a constant work distribution also leads to very long chords at the hub, which makes the width of the fan too large. Hence, it is inappropriate for automotive cooling applications. For these reasons, different blade variants with non-constant radial work distributions have been designed with the airfoil theory approach and the influence of these work distributions on the performance and efficiency characteristics of the fan have been analyzed

DESIGN PROCEDURE

In the present case, the volumetric air flow rate, the total-to-static pressure and the shroud diameter were fixed. Regardless of which design approach is used, the velocity triangles at several radial blade sections must be determined. Thereby in the design stage it is assumed, that the incoming airflow is swirl-free ($c_{u1}=0$) and the meridional and circumferential velocities at each radius are equal from the inlet to the outlet. Furthermore, the air is assumed to be incompressible, which is reasonable with Mach numbers below 0.3. To be able to fully determine the velocity triangles, additional conditions are required. By figuring out the optimal rotational speed for the present rotor, the circumferential velocity u can be calculated. Therefor the diameter coefficient

$$\delta = \frac{\sqrt{\pi}}{2} d_{shroud} \sqrt[4]{\frac{2Y}{\dot{V}^2}} \tag{1}$$

has been calculated and the optimal speed coefficient

$$\sigma = 2\sqrt{\pi}\, n \frac{\sqrt{\dot{V}}}{(2Y)^{3/2}} \tag{2}$$

has been determined using the Cordier diagram. Based on this speed coefficient the rotational speed for the design point was calculated with eq. (2). The design point finally was given by a volumetric flow rate of Q = 0.3 m³/s, a total pressure of dp_t = 260 Pa and a rotational speed of n = 5000 1/min.

The radial equilibrium of the centrifugal and the static pressure forces

$$\frac{dp_{s2}}{dr} = \rho \frac{c_{u2}^2}{r} \tag{3}$$

provides the second condition to determine the meridional velocity c_m. It can be expressed by the velocity components of the velocity triangles and their radial differentiations in the following way

$$\omega \frac{d(c_{u2} r)}{dr} = \frac{c_{u2}}{r} \cdot \frac{d(c_{u2} r)}{dr} + c_m \frac{dc_m}{dr} \tag{4}$$

For the detailed transformation from eq. (3) to eq. (4) see Carolus [1]. By defining a radial work distribution, c_{u2} can be determined using the Euler equation

$$Y = \frac{\Delta p_t}{\rho} = u\, c_{u2} \tag{5}$$

Afterwards eq. (4) can be numerically solved for several radial sections, which results in a meridional velocity c_m-distribution. In this way, all velocity components can be calculated for each blade section. Afterwards the overall volume flow rate,

hydraulic power, total pressure rise and total to static pressure rise can be determined by integration with the following equations:

$$\dot{V} = 2\pi \int_{r_{hub}}^{r_{tip}} c_m \, r \, dr \tag{6}$$

$$P_{hyd} = 2\pi \, \omega \, \rho \int_{r_{hub}}^{r_{tip}} c_m \, r^2 \, c_{u2} \, dr \tag{7}$$

$$\Delta p_t = \frac{P_{hyd}}{\dot{V}} \tag{8}$$

$$\Delta p_{t-s} = \Delta p_t - \frac{\pi \, \rho}{\dot{V}} \int_{r_{hub}}^{r_{tip}} r \, c_m \, (c_m^2 + c_{u2}^2) \, dr \tag{9}$$

The fundamental process in the airfoil approach is the calculation of the solidity, e.g.

$$\frac{l}{t} = \frac{2Y}{c_l \, w_\infty \, u \left(1 + \frac{\varepsilon}{\tan \beta_\infty}\right)} \tag{10}$$

with the absolute value of the vectorial average of the relative flow velocities at the inlet and the outlet

$$w_\infty = \left|\frac{1}{2}(\vec{w}_1 + \vec{w}_2)\right| = \frac{1}{2}\sqrt{\left(u + \sqrt{w_2^2 - c_m^2}\right)^2 + 4c_m^2} \tag{11}$$

has been selected.

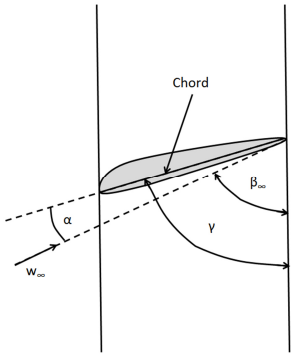

Figure 1: Stagger angle γ

The airfoil characteristics were determined using the airfoil analysis and design software Xfoil, developed at the MIT by Mark Drela [4], since for most airfoils data is available only for a small amount of different Reynolds numbers. For the present case, a NACA 5506 airfoil was selected. NACA airfoils are parametrized and can therefore be easily modified. Moreover, NACA airfoils can automatically be created by the turbomachinery design software CFturbo [5], which was used to create the CAD-models of the calculated blade designs.

and the corresponding flow angle

$$\beta_\infty = \tan^{-1}\left(\frac{2c_m}{u + \sqrt{w_2^2 - c_m^2}}\right) \tag{12}$$

For the derivation of eq. (10) see Carolus [1] and Bohl [3]. Multiplying eq. (10) by the blade spacing

$$t = \frac{2\pi r}{z} \tag{13}$$

results in the chord length l for the current radius. The values of the lift coefficient c_l and the drag/lift ratio ε in eq. (10) depend on the characteristics of the selected airfoil and the Reynolds number

$$R_e = \frac{w_\infty l}{\nu} \tag{14}$$

The Reynolds number in turn depends on the chord length l, which is the outcome of eq. (10). For this reason, an iterative solver is required, to calculate the chord lengths of each radial section. The angle of the blades is defined as the stagger angle

$$\gamma = \beta_\infty + \alpha \tag{15}$$

between the chord of the airfoil and the front of the blade section, Figure 1. Based on the airfoil characteristics, the angle of attack which results in the minimal drag/lift ratio at each blade section

Thus, a data conversion of the point based airfoil geometry files was not necessary. The NACA 4-digit series allows adjusting the camber and the thickness independently of each other. In this way, it was possible to define a low camber, which is suitable for the low Reynolds numbers occurring at the present rotor, while keeping a proper thickness to maintain manufacturability.

The number of blades and the hub diameter are not directly determined by these calculations. Generally, many blades create more friction losses while too few blades lead to high blade loading and thus larger losses due to secondary flows. For the present case, the recommendation of 7 blades was adopted from CFturbo. Higher hub to shroud diameter ratios generally result in higher pressure rises and lower flow rates, since the pressure rise occurs at higher radii and the cross section is smaller [6]. For the same flow rates the meridional velocities have to be higher since the cross-section area is smaller. This is also the reason why the friction losses also rise with higher hub to shroud diameter ratios, which is not considered in the calculations above. Hence, the hub diameter was specified by stepwise increasing the hub to shroud diameter ratio starting at 0.25, until the desired total to static pressure rise was achieved according to eq. (9).

RADIAL WORK DISTRIBUTIONS

As mentioned before, CFturbo was used for the creation of the CAD-Models of the fan blades. At first, an initial design with constant radial work distribution was created, since this is the standard setting of CFturbo and especially because the constant work design is in general very often used. One issue of this design is that it results in high solidity values near the hub. The airfoil approach is only applicable, if the blades stand sufficiently far apart and have little influence on each other. This means, that the rotor needs to have a small solidity. CFturbo recommends using the standard airfoil approach up to a solidity of 0.68. For rotors with a higher solidity it is recommended to use the Lieblein method [1] which complements the airfoil approach with the use of empirical data and is applicable for solidities between 0.4 and 2.0. Figure 2 shows the resulting deflection $\Delta\beta = \beta_2 - \beta_1$ and the solidity for 15 equidistant radial blade sections calculated by CFturbo and by manually applicating the equations described in the previous section. CFturbo basically uses the same equations, but also incorporates the blockage of the blades, which leads to higher meridional flow velocity. Since there is always a specific relation between the chord length and the thickness of a blade section, the long chords at the hub are also very thick. Hence, the CFturbo calculation differs strongly from the manual calculations at the hub. Both calculations result in a solidity that exceeds the limit of 0.68 near the hub. Also, it falls below the minimum of 0.4 which is required for the application of the Lieblein method, near the shroud. The long chords resulting from the high solidity and the small number of blades require a wide hub and thus additional weight and installing space. Hence, this design is inappropriate for automotive cooling applications, especially for a race car where the weight of the car is an important issue. The high deflection angles near the hub cause high blade loadings. Especially the $\Delta\beta$-values calculated by CFturbo, which is considered being more accurate than the manual calculations, can lead to losses due to flow separation and secondary flows.

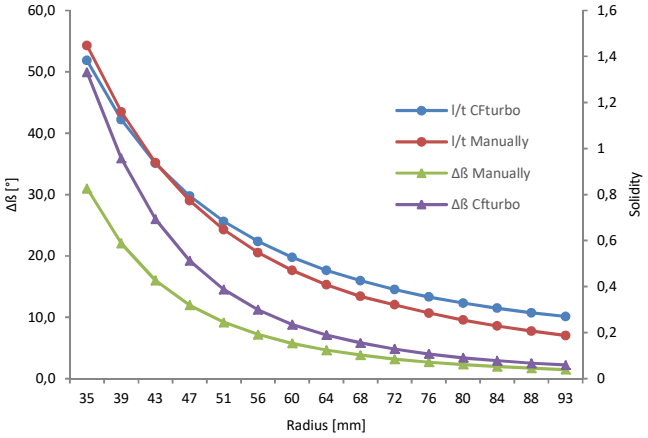

Figure 2: Deflection angles and solidity for constant work distribution

These issues can be avoided by increasing the hub to shroud diameter ratio. But to achieve a solidity below 0.68 in this way, the hub to shroud diameter ratio would need to be increased from the current value 0.38 to 0.59. As described in the previous section, this would result in higher pressure rise and friction losses. Since the additional pressure rise is not usable in the present application, different radial work distributions have been specified. The specified work distributions are shown below in Figure 3.

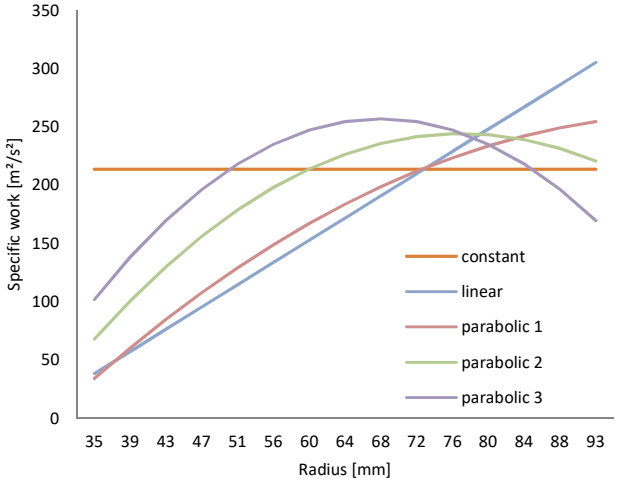

Figure 3: Specified radial work distributions

The alternative designs include one linear and three parabolic work distributions. The parabolic work distributions have their maximum at different radii. The overall work, resp. total pressure rise resulting from eq. (7) and (8) is the same with all work distributions. Although CFturbo allows slight adjustments on the c_{u2}-distribution, it does not support this kind of inverse design. Hence, the alternative designs were calculated manually and the results were entered into CFturbo in order to generate CAD-models. This means, that the blockage effect of the blade is neglected, which is considered being reasonable, because the chords of the alternative designs are much shorter and therefore thinner than the blades of the constant work design. The deflection angles and the solidity of the alternative work distributions are shown below in Figure 5 and Figure 6.

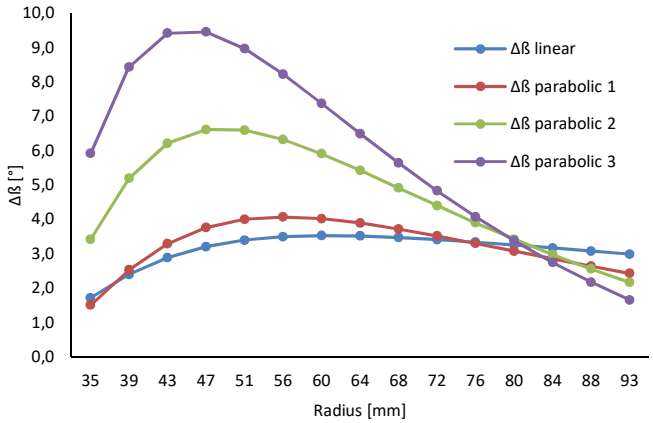

Figure 4: Deflection angles of the non-free vortex designs

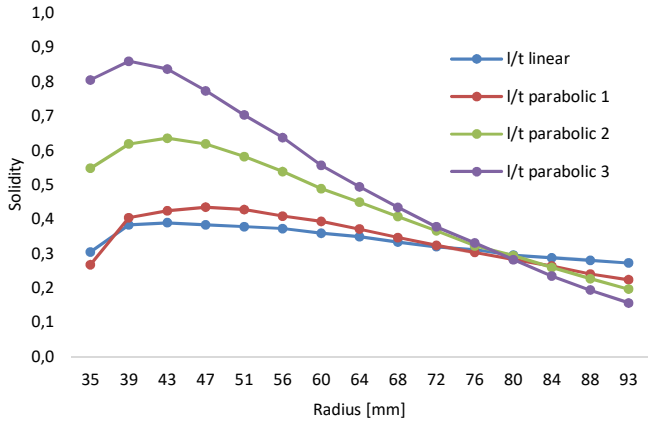

Figure 5:Solidity of the non-free vortex designs

SIMULATION SETUP

The designs described in the previous section have been analyzed with the commercial CFD software Star CCM+. The simulation setup consists of three cylindrical regions with the same diameter in a row – the inlet region, a cylinder surrounding the fan geometry and the outlet region. In order to incorporate the tip losses, the diameter of these regions is slightly larger than the shroud diameter of the fan. The front surface of the inlet region is defined as a mass flow inlet boundary condition, where different mass flows were specified in order to simulate multiple operation points. The back surface of the outlet region is defined as a pressure outlet with 0 Pa, which is the global reference pressure. The lateral surface of the fluid regions and the surface of the fan geometry are specified as no slip walls. In axis symmetric applications like this the frozen rotor approach can be used. This means that steady state simulations have been computed and the region surrounding the fan has been assigned to a rotating reference frame, so that in this region the centrifugal and Coriolis forces are added to the momentum equations. This method needs significantly less time and computational power than a transient simulation. Moreover, constant density has been assumed, which is adequate for low pressure fans. For turbulence modelling the SST model of Menter has been used, since this is the current industrial standard model.

The rotating region was meshed with polyhedral cells, since the Star CCM+ documentation recommends this mesh model for general purposes with complex flows. For the inlet and outlet region a simpler trimmed hexahedral mesh was used. The mesh of the rotating region has been refined around the surfaces of the fan blades. To determine an appropriate mesh density, a mesh study has been done. Therefore, the total pressure and the torque have been evaluated at simulations with different mesh densities. The mesh study (fig. 6) shows that the results start to converge at a mesh size of about one million grid cells. The results of the simulations with at least one million grid cells differ around 5% (total pressure) resp. 3 % (torque).

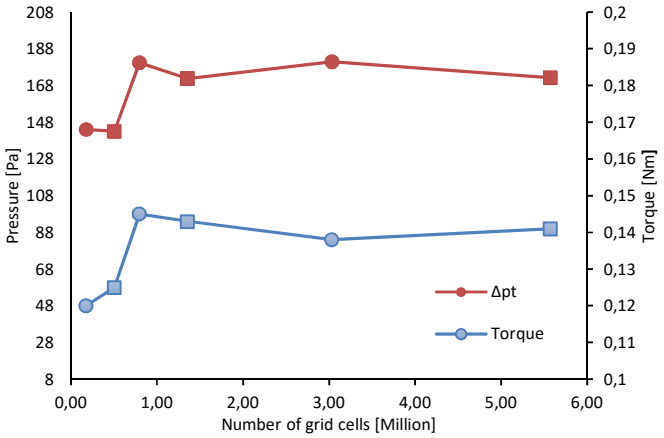

Figure 6: Results of the mesh study

In the simulations marked with a square, prism layers have been used at the blade surfaces. For the following simulations, a grid size of 3 Million cells was chosen.

RESULTS

The characteristics resulting from the simulation Figure 7 - Figure 10 show that contrary to the expectations the design with the constant work distribution has the highest total efficiency of all designs and also delivers the second highest total pressure. Compared to the other designs, however, it delivers only a poor total-to-static pressure. The design with the linear work distribution delivers the highest total pressure, total-to-static efficiency and thus also the highest total-to-static pressure. Yet, the total efficiency of this design is clearly below the constant work design. The first parabolic work distribution delivers the lowest values in all performance parameters, although it is very similar to the linear work distribution.

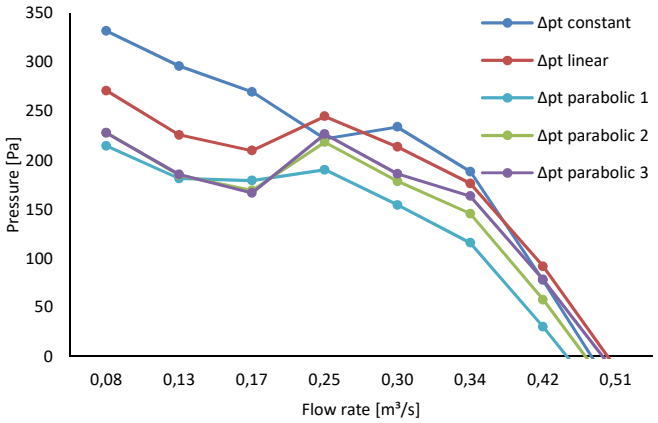

Figure 7: Total pressure characteristics

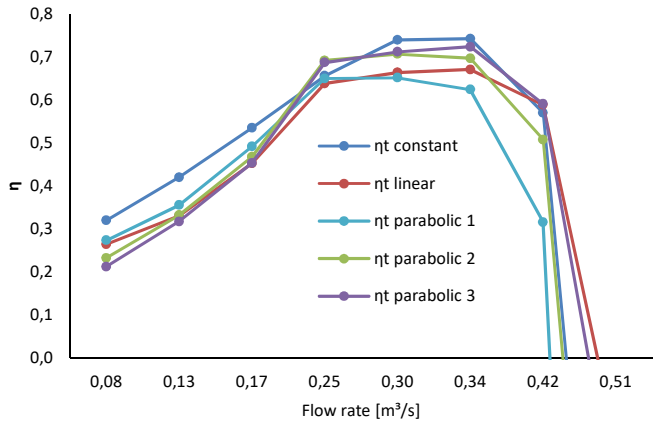

Figure 8: Total efficiency characteristics

In order to further analyze these results the predefined work distributions of each design have been compared to the work distributions resulting from the simulation. Therefore, the mass flow averaged total pressure at several ring sections of equal cross sectional area has been read out. Thereby, only the work distribution of the linear design Figure 11 agrees with the predefined work distribution. The other simulated work distributions are significantly below the predefined work distributions, Figure 12 - Figure 15. This explains, why the design with linear work distribution delivers the highest total and total-to-static pressure. The first design with parabolic work distribution delivers poor performance, because its work near the hub is below the already very low predefined values. Also, it does not reach the high predefined work values near the shroud. This results in an overall low work and thus low total and total-to-static pressure.

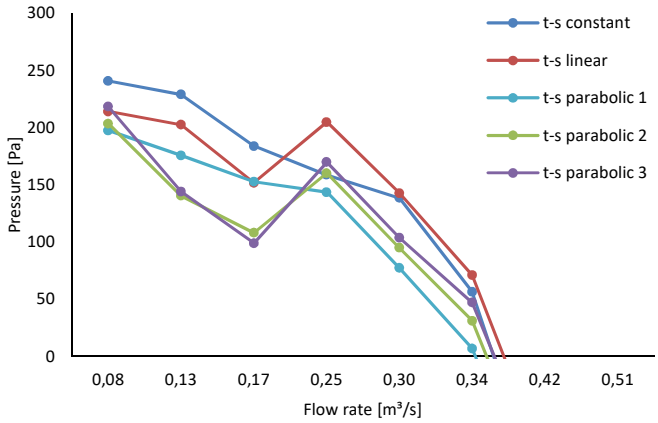

Figure 9: Total-to-static pressure characteristics

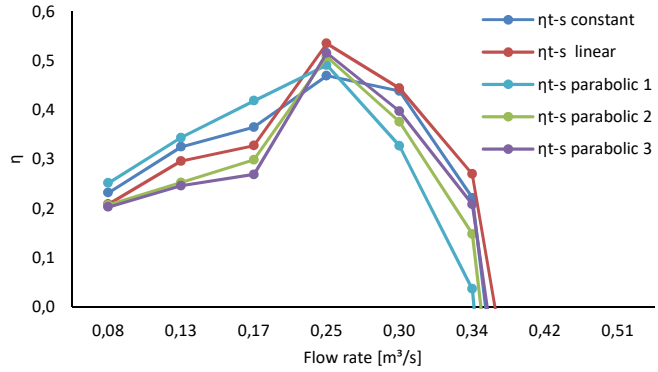

Figure 10: Total-to-static efficiency characteristics

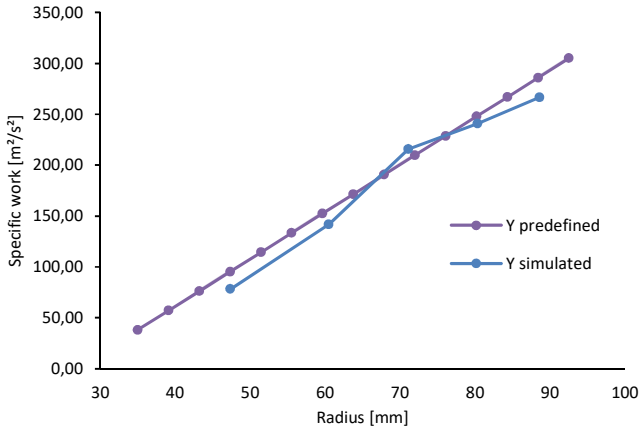

Figure 11: Linear work distribution, predefined and simulated

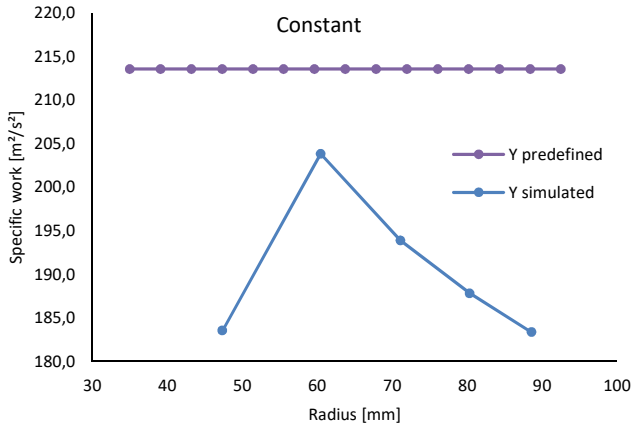

Figure 12: Constant work distribution, predefined and simulated

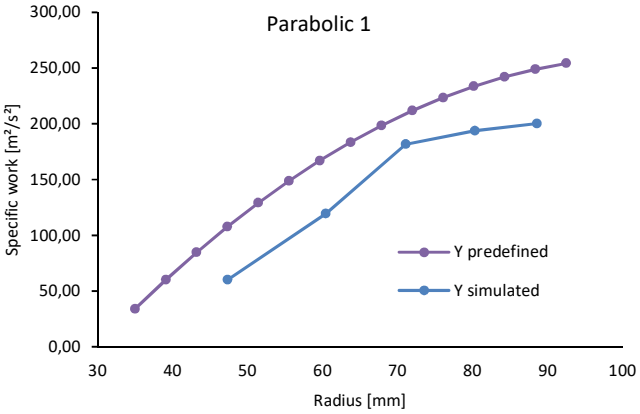

Figure 13: First parabolic work distribution, predefined and simulated

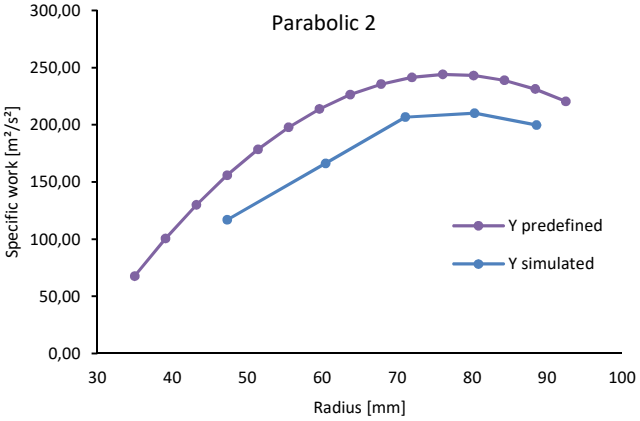

Figure 14: Second parabolic work distribution, predefined and simulated

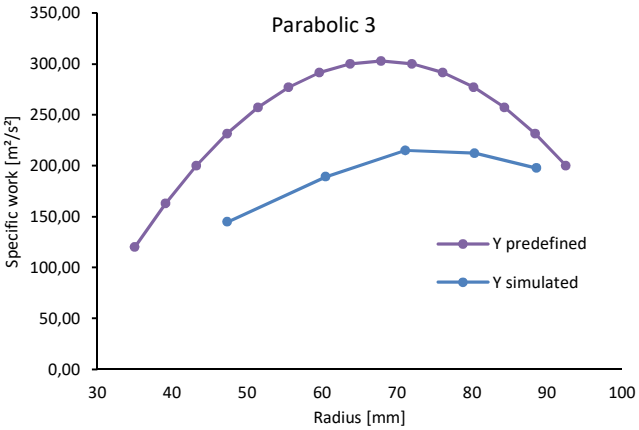

Figure 15: Third parabolic work distribution, predefined and simulated

In Figure 16 to Figure 20 the theoretical and the simulated meridian velocities are shown. The simulated meridional velocities agree with the theoretical values at midspan. Near the shroud, they drop far below the theoretical values, which can be explained by losses due to blade tip leakage.

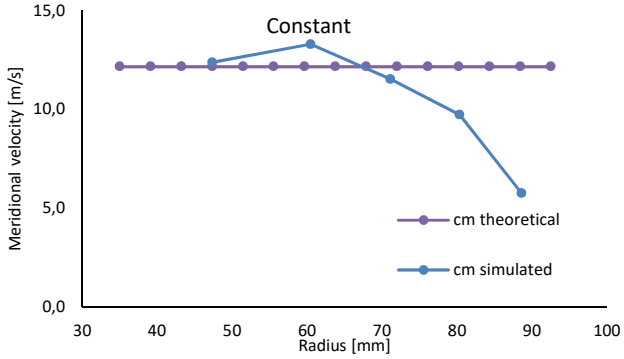

Figure 16: Constant work distribution, predefined and simulated meridian velocity

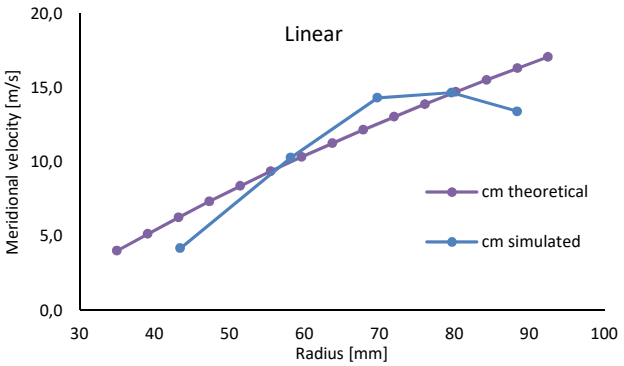

Figure 17: Linear work distribution, predefined and simulated meridian velocity

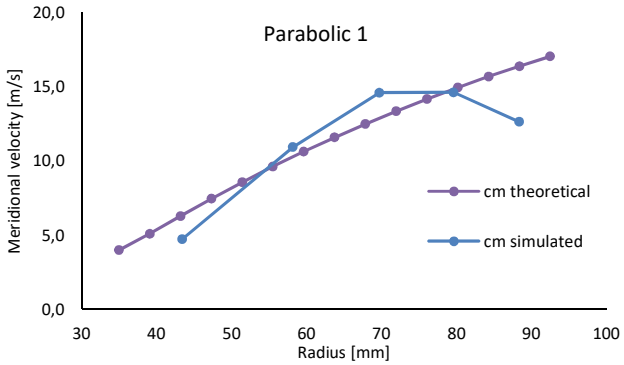

Figure 18: First parabolic work distribution, predefined and simulated meridian velocity

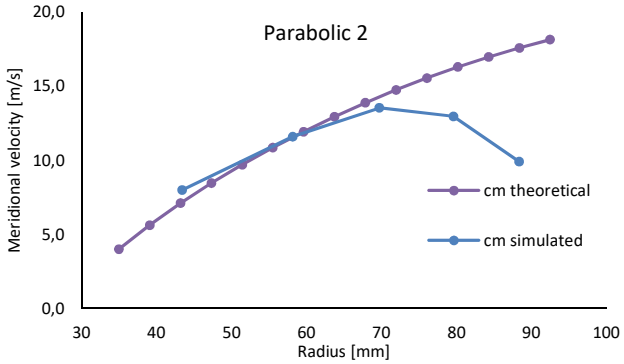

Figure 19: Second parabolic work distribution, predefined and simulated meridian velocity

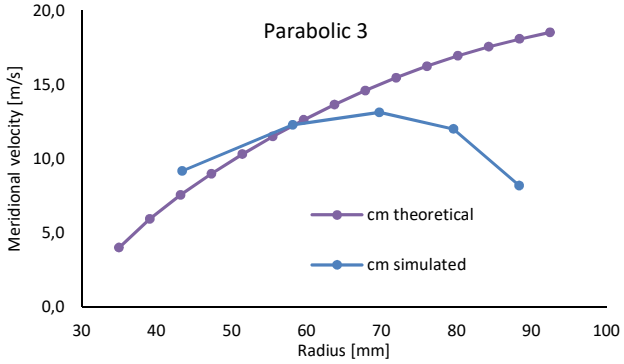

Figure 20: Third parabolic work distribution, predefined and simulated meridian velocity

The simulations presented above are comparable with the measurements carried out by Vad and Bencze **[7]**. They investigated three axial fans with linear radial work distributions with different gradients. They found that their measured data only agree with the theoretical values at one fan. Also they obtained a steep drop of the meridional velocity near the shroud. These results agree qualitatively with the results of the present work.

CONCLUSIONS AND OUTLOOK

Based on the characteristics and the simulated radial work distributions, a correlation between the radial location of the major work and the behavior of the fan can be derived. Allocating large amounts of work near the shroud radius leads to high total and total-to-static pressure and also to a high total-to-static efficiencies, while allocating large amounts of work near the hub leads to low pressures and total-to-static efficiency but also in a high total efficiency. The losses of designs with much work at the shroud radius can be explained by the higher tip losses due to the higher blade loading at the shroud radius. Relocating work from the hub to the shroud is basically equivalent to increasing the hub to shroud diameter ratio. This confirms the declaration, that a high hub to shroud diameter ratio leads to a high pressure but a low total efficiency and a low hub to shroud diameter ratio leads to a low pressure and high total efficiency.

The comparison of the performance and efficiency characteristics show that the free vortex design is the best choice, only if a high total efficiency is the main objective, although it is not able to realize the full predefined work in this case. The high blade loading at the hub of this design did not cause as much flow separation as expected. The wall shear stress contour plots in the annex show, that all designs have minor separations at the hub, but generally work well. This explains the common usage of the free vortex design. For automotive cooling purposes, however, a design with more work at the shroud region is better, because it results in a higher total-to-static pressure as well as a higher total-to-static efficiency, with the same diameter, rotational speed and design volume flow. For fan applications the total-to-static pressure and the total-to –static efficiencies are in general the relevant parameters, since the dynamic pressure at the exit is lost in almost all fan applications. Therefore, depending of the application, a design with more work at the shroud may have clear advantages over the free vortex design. Also, it leads to short chords at the hub and thus in narrow fans requiring less space for installation.

The simulations presented in this paper will be further investigated.. In future studies it will be be studied, why the actual work agrees with the theoretical values for one work distribution only and how such an agreement can be achieved. Possibly a maximum blade loading and hence work for each radius can be determined.

REFERENCES

[1] T. Carolus, Ventilatoren, Wiesbaden: Springer Vieweg, 2013.

[2] B. Eck, Ventilatoren, Heidelberg: Springer Verlag, 2003.

[3] W. Bohl and W. Elmendorfer, Strömungsmaschinen 1: Aufbau und Wirkungsweise, 11. Auflage ed., Würzburg: Vogel Business Media, 2012.

[4] XFOIL, http://web.mit.edu/drela/Public/web/xfoil/, 2013.

[5] CFturbo, http://de.cfturbo.com/home.html, 2017.

[6] P. Epple, F. Durst and A. Delgado, "A theoretical derivation of the Cordier," *Proceedings of the Institution of Mechanical Engineers, Part C: Journal of Mechanical Engineering Science,* 2011.

[7] J. Vad and F. Bencze, "Three-dimensional flow in axial flow fans of non-free vortex design," *International Journal of Heat and Fluid Flow,* 1998.

[8] B. Eck, Fans - Design and Operation of Centrifugal, Axial-Flow and Cross-Flow Fans, Oxford: Pergamon Press Ltd., 1972.

[9] L. Somlyódy, Wirkung der Drallverteilung auf die Kenngrößen von Axialventilatoren, Technische Universität Budapest, Lehrstuhl für Wasserkraftmaschinen, 1970.

ANNEX: CONTOUR PLOTS OF THE WALL SHEAR STRESS OF THE ANALYZED DESIGNS

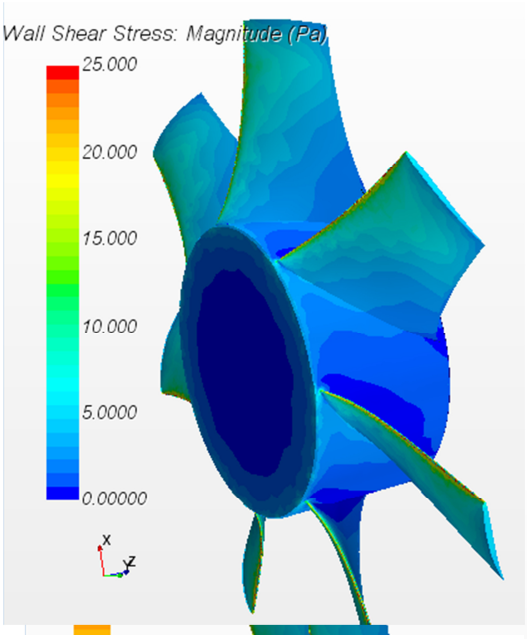

Constant

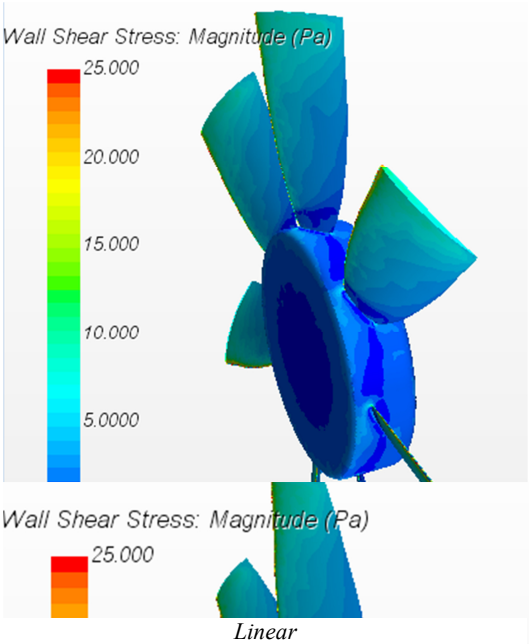

Linear

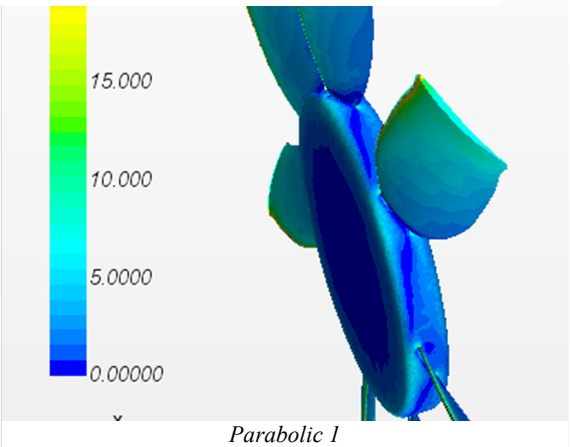

Parabolic 1

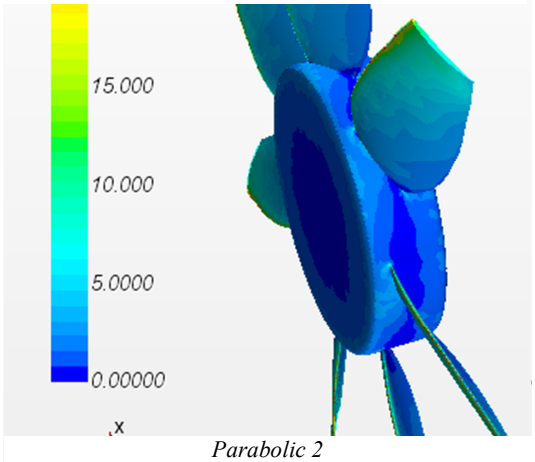

Parabolic 2

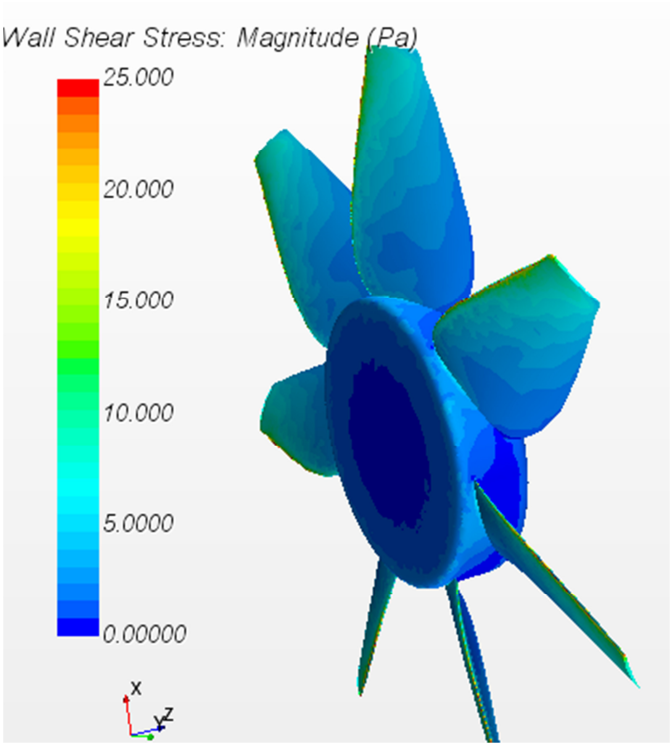

Parabolic 3